100
3-15-94 JSO

DOE/BC/14899-9
(DE94000116)

VISUALIZATION AND SIMULATION OF BUBBLE GROWTH IN PORE NETWORKS

Topical Report

By
Xuehai Li
Yanis C. Yortsos

March 1994

Performed Under Contract No. DE-FG22-93BC14899

University of Southern California
Los Angeles, California

Bartlesville Project Office
U. S. DEPARTMENT OF ENERGY
Bartlesville, Oklahoma

DISCLAIMER

This report was prepared as an account of work sponsored by an agency of the United States Government. Neither the United States Government nor any agency thereof, nor any of their employees, makes any warranty, expressed or implied, or assumes any legal liability or responsibility for the accuracy, completeness, or usefulness of any information, apparatus, product, or process disclosed, or represents that its use would not infringe privately owned rights. Reference herein to any specific commercial product, process, or service by trade name, trademark, manufacturer, or otherwise does not necessarily constitute or imply its endorsement, recommendation, or favoring by the United States Government or any agency thereof. The views and opinions of authors expressed herein do not necessarily state or reflect those of the United States Government or any agency thereof.

This report has been reproduced directly form the best available copy.

Available to DOE and DOE contractors form the Office of Scientific and Technical Information, P.O. Box 62, Oak Ridge, TN 37831; prices abailable form (615) 576-8401.

Available to the public from the National Technical Information Service, U.S. Department of Commerce, 5285 Port Royal Rd., Springfield VA 22161

DOE/BC/14899-9
Distribution Category UC-122

Visualization and Simulation of Bubble Growth in Pore Networks

Topical Report

By
Xuehai Li
Yanis C. Yortsos

March 1994

Work Performed Under Contract No. DE-FG22-93BC14899

Prepared for
U.S. Department of Energy
Assistant Secretary for Fossil Energy

Thomas B. Reid, Project Manager
Bartlesville Project Office
P.O. Box 1398
Bartlesville, OK 74005

Prepared by
University of Southern California
Petroleum Engineering Department
Department of Chemical Engineering
Los Angeles, CA 90089-1211

MASTER

CONTENTS

List of Figures

ABSTRACT

Bubble nucleation and bubble growth in porous media is an important problem encountered in processes, such as pressure depletion and boiling. To understand its basic aspects, experiments and numerical simulations in micromodel geometries were undertaken. Experiments of bubble growth by pressure depletion were carried out in 2-D etched-glass micromodels and in Hele-Shaw cells. Nucleation of bubbles and the subsequent growth of gas clusters were visualized. Contrary to the bulk or to Hele-Shaw cells, gas clusters in the micromodel have irregular and ramified shapes and share many of the features of an external invasion process (e.g. of percolation during drainage). A pore network numerical model was developed to simulate the growth of multiple gas clusters under various conditions. The model is based on the solution of the convection-diffusion equation and also accounts for capillary and viscous forces, which play an important role in determining the growth patterns. Numerical simulation resulted in good agreement with the experimental results.

INTRODUCTION

Bubble nucle ation and bubble growth during pressure depletion in porous media is an important problem encountered in processes, such as solution gas-drive and boiling. The first is typical of oil recovery methods from underground reservoirs, when the reservoir pressure falls below the bubble point.[1] The second is common to enhanced boiling heat transfer,[2] geothermal energy processes[3] and other applications.[4] More generally, these problems involve important aspects of phase change in porous media. Here, the interaction between the pore microstructure and transport and capillary phenomena adds many novel aspects to the growth of the new phase, which are absent from the same processes in the bulk or from external displacements in porous media.[5-7] Bubble growth in porous media is still not fully understood and many problems, both theoretical and practical, remain unresolved. In solution-gas drive processes, which are of main interest here, these include the value of the *critical gas saturation*, S_{gc}, which denotes the minimum gas volumetric content before the onset of bulk gas flow, and the effect of pressure decline rate on growth.[8-10] Their consideration is important for the optimal design of various oil recovery methods, particularly in fractured systems, where the solid matrix has low permeability.[11] Analogous problems exist in boiling. In either application, the state of the art is mostly phenomenological, and it is typically based on the use of various forms of effective medium approximations.

In this paper we will restrict our attention to the growth of a single-component gas from a saturated two-component liquid, driven by a decline in the liquid pressure. Related work on the boiling problem is currently in progress.[12] Previous research on these problems has been inconclusive.[1,13,14] Early attempts focused mostly on nucleation characteristics,[1,13] with only limited attention paid to the subsequent growth. Particularly controversial is the effect of pressure decline rate. Some authors have used expressions from homogeneous nucleation to surmise effects of pressure decline on the overall growth process.[13] Others have applied concepts from bubble growth in the bulk, using compact, non-interacting bubbles to describe gas phase growth.[15,16] Experimental support for porous media processes has been limited. Most experiments in laboratory cores are typically interpreted based on an integrated response of the system rather than *in situ* observations. This approach is inherently inadequate to resolve important small scale issues.

In a recent study[17] we provided the first model that emphasized the effect of pore structure in controlling the growth patterns and postulated the existence of percolation-like gas clusters. We proceeded by separating nucleation from bubble growth. From an analysis of the nucleation problem, we postulated that the occupancy of a pore, which for all practical purposes signals the onset of observable nucleation, is controlled by capillary heterogeneities in the pore surface (e.g. cavities) that trap gas microbubbles. We then proceeded to relate the onset of nucleation to the condition that the local supersaturation exceeds their capillary barrier. For example, assuming a nucleation site (cavity) of width W, the critical supersaturation for its activation would be $\Delta P \equiv KC - P_l \sim \frac{2\gamma}{W}$, where K is the solubility constant, C and P_l denote local concentration and liquid pressure, respectively and γ is the interfacial tension. According to this model, therefore, the effect of the pressure decline rate would be in activating such sites rather than in modifying the kinetics of homogenous nucleation, as previously postulated. Similar conclusions on the role of surface heterogeneities were reached in a more recent experimental study by Yousfi et al.[18]

Yortsos and Parlar[17] also formulated the equations for bubble growth in porous media and proceeded with a qualitative delineation of the various patterns. However, they were able to obtain quantitative results only in the limiting case of very low supersaturations, where concentration gradients are weak and the process is controlled only by capillary forces. A condition on the pressure decline rate was derived for this regime to be applicable. Under this condition, the problem can be approached as invasion percolation from multiple internal growth sites. The analysis shows that the gas saturation is then only a function of pressure and of the of the fraction of activated sites. The importance of capillarity and the possible emergence of a percolation regime were qualitatively verified in preliminary experiments by Yousfi et al.[19], who studied the liberation of CO_2 gas from supersaturated carbonated water in micromodels. Their results confirmed the existence of specific nucleation sites and the subsequent growth of gas bubbles in the form of ramified clusters. Visualization studies of solution gas-drive at high pressure and temperature were also conducted by Danesh et al.[20], with the use of organic compounds. These authors focused on the onset of nucleation, which also occured in specific sites (which happened to coincide with the largest pore body), and on certain local mechanisms of growth.

While these studies offered much insight in the micromechanics of the process, a host of questions still remain unanswered. For example, the simple theory of Yortsos and Parlar[17] does not address effects of pressure decline rate on bubble growth, the type and growth rates of the various patterns, or the competition between growing clusters. In the analogous problem of phase growth in the bulk, competition between growing compact (spherical) particles is usually subject to Ostwald ripening,[21] the larger sizes growing at the expense of the smaller ones. A different mechanism is expected in porous media, where due to the microstructure, the local gas-liquid curvature is unrelated to the cluster size. Of much interest also are process scale up and finite size effects.

In a recent investigation, described in the companion publications,[22-24] we have revisited the problem of bubble growth in porous media. Li and Yortsos[22] considered bubble stability in an *effective* porous medium, where a new stabilizing mechanism on the growth of the new phase was identified. That study has relevance to the delineation of growth patterns in effective media, such as a Hele-Shaw cell, where the local microstructure is absent. The effect of microstructure was emphasized in [23] and [24]. Scaling laws for the growth of a single cluster were proposed in [23], while a general theory for growth of multiple clusters was formulated in [24]. These two theoretical studies rely on experimental observations and numerical simulations described in this paper. Here, we report on visualization experiments, conducted in etched glass micromodels, as described in Yousfi et al.[19], and in Hele-Shaw cells. The growth of a gas phase from a supersaturated carbonated water solution, driven by a pressure decline, is studied. In particular, we focus on nucleation aspects, the mode of pore occupancy and the effect of the pressure decline rate. Subsequently, a pore network is developed to describe gas phase growth. Finally, the experiments are simulated with the use of the pore network model.

EXPERIMENTS

To obtain an insight on the micromechanics of bubble growth, visualization experiments were conducted. Following Yousfi et al.[19], we considered the liberation of CO_2 gas from saturated carbonated water contained in an etched-glass micromodel. The micromodel was prepared by etching a 2-D square network pattern of pores and throats on a glass plate (Figure 1) which was subsequently fused to another glassplate to create a 2-D pore network. Details of

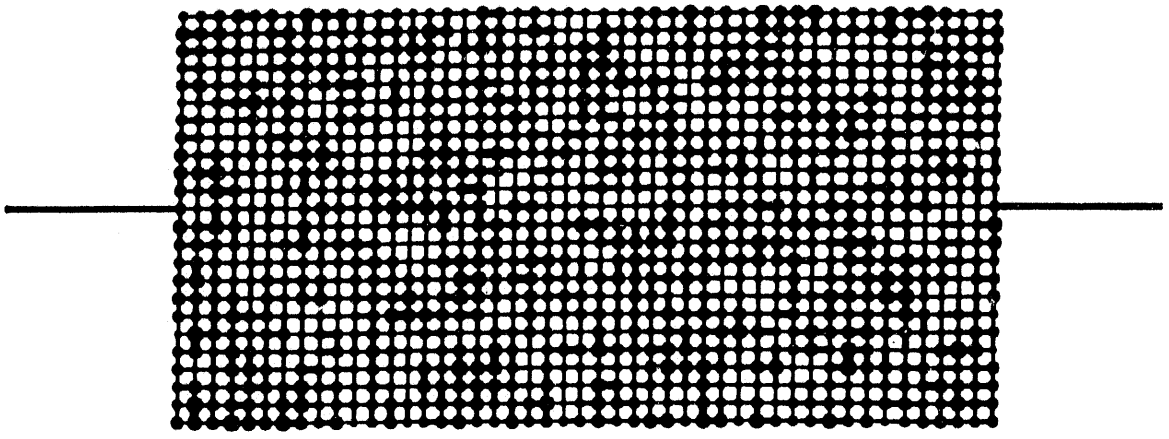

Figure 1. Schematic of pore network and glass micromodel pattern.

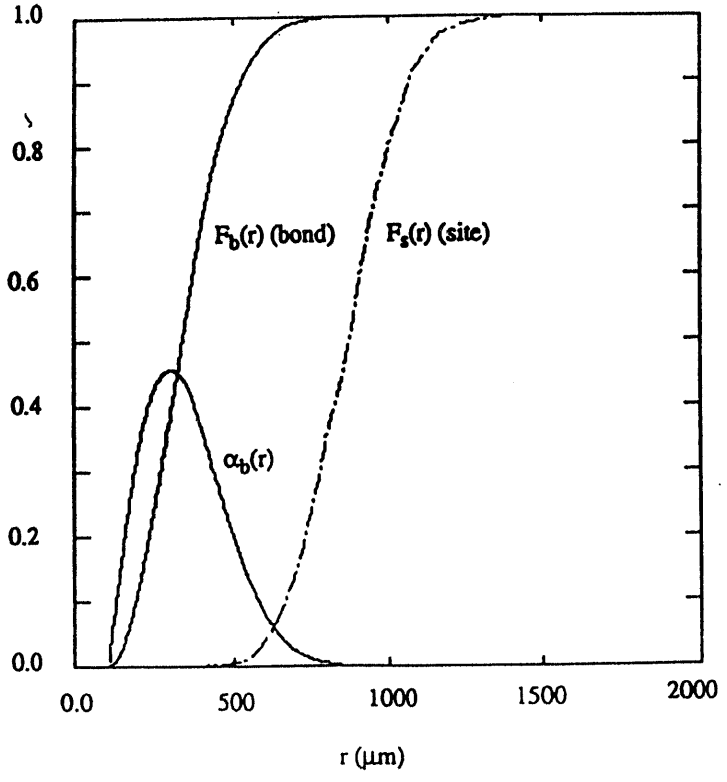

Figure 2. Rayleigh distributions of pore throat (bond) and pore body (site) sizes.

the fabrication process can be found in [25]. Pore throat and pore body size distributions were selected from the Rayleigh distribution shown in Figure 2. Due to imperfections in the glass and the lack of precise control in etching and fusion, however, the final pattern is not identical to the original. As will be shown below, this places limitations on the ability to exactly reproduce the experimental results by numerical simulation. For comparison purposes, experiments were also conducted in a Hele-Shaw cell, which was constructed from two parallel glass plates of dimensions 2.5×10 cm separated by a spacing of 200 μm. The schematic of the experimental setup is shown in Figure 3. A helium gas tank and a flow controller were used to control the pressure decline rate. The experimental procedure was as follows:

(1) CO_2 gas was first injected to displace air from the glass micromodel or the Hele-Shaw cell.

(2) Subsequently, distilled water was injected at a high pressure, typically around 60 psi to saturate the micromodel.

(3) Supersaturated carbonated water was injected along with a coloring dye to displace the distilled water. We typically used a saturation pressure of 50 psi and a supersaturation of 5-30 psi.

(4) The micromodel was connected to the helium gas tank and the system pressure was reduced at the specified decline rate by releasing helium gas.

(5) The process was videotaped and the system pressure was recorded.

Shown in Figure 4 is a typical sequence of bubble growth in the glass micromodel for a pressure decline rate of 8.64 psi/hr. The onset of growth occurs from various nucleation sites, which become activated at different stages of the process, usually after a certain supersaturation level was reached. A wide range of supersaturations for different systems has been reported in the literature.[11,26–28] In our glass micromodel experiments, we observed supersaturations varying from 5 psi to 30 psi. This is consistent with cavity sizes W of the order of 1-10 μm. Occasionally, we were able to observe an activation event. The sequence of

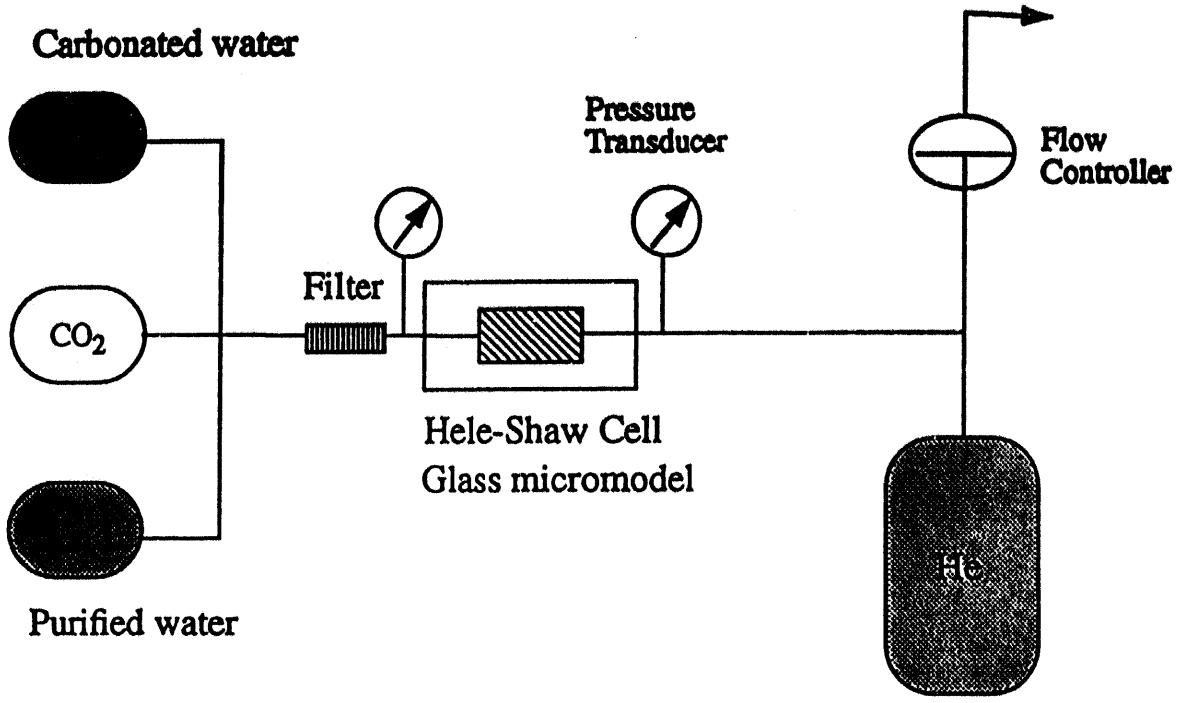

Figure 3. Schematic of the experimental apparatus.

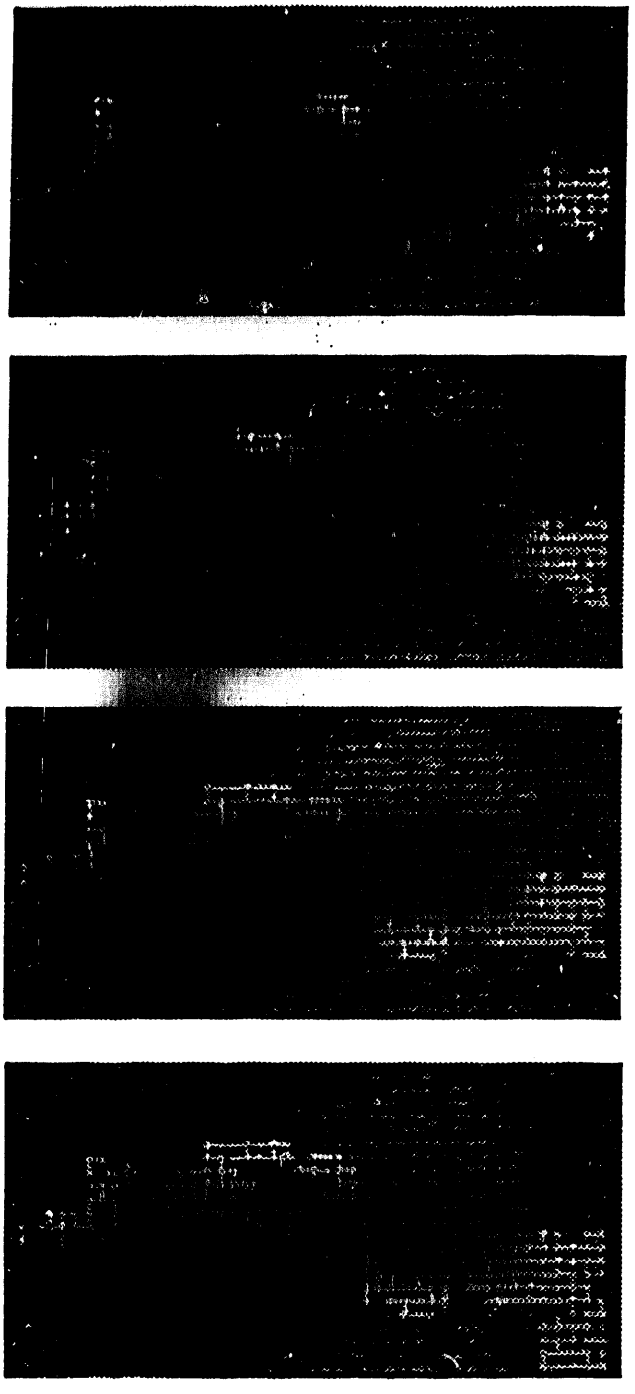

Figure 4. Snapshots of growth patterns in the glass micromodel at a pressure decline rate of 8.64 psi/hr.

Figure 5 shows the detachment from the surface and the sunsequent growth of a microbubble, originally trapped at pore surface heterogeneities. The time elapsed from the macroscopic appearance of the microbubble (first frame) to its detachment, growth and subsequent occupancy of the pore body (last frame) is of the order of a few seconds, suggesting that for practical purposes one can identify the condition for the occupancy of a pore body with that for the release of the trapped microbubble from a surface cavity. Although of heterogeneous origin, however, nucleation was not reproducible. We suspected that this was due to the injected dye particles which acted as nucleation sites. The frequency of nucleation decreased substantially when the experiments were carried out in the absence of dye.

Subsequent to nucleation, gas clusters begin to grow in an irregular, often ramified, fashion (Figure 4). Trapping of the displaced liquid phase, which is characteristic of invasion percolation processes in external displacement, was frequently observed. A typical sequence of the growth of a gas cluster shown in Figure 6 involves two steps: (i) A slow pressurization step, during which the pressure in the cluster increases and the gas-liquid menisci move only slightly to adjust their curvature to the pore geometry; and (ii) A fast penetration step (similar to "rheon" events in drainage[29]) immediately after a capillary barrier at a perimeter throat is exceeded. In all our experiments, which involve pressure decline rates in the range $0.1 - 60\ psi/hr$, cluster growth occured by penetration of only one perimeter throat per cluster at a time. Following this step, the volume of the cluster increased, as the new invaded site became occupied, while further slight adjustment of all interfaces was noted. This sequence was repeated in the next event. By contrast, in experiments involving Hele-Shaw cells, although also initiated from different nucleation sites, the gas clusters grow in a compact, almost perfectly radial fashion, following a macroscopically smooth movement (Figure 7). Bubble coalescence eventually produces large non-radial clusters, however, the patterns remain compact at all times. The difference between the two growth patterns is due to the microstructure of the glass micromodel. A similar difference is also found in typical external displacements (e.g. compare viscous fingering patterns in Hele-Shaw cells and in porous media[30]), and can be analyzed using statistical physics theories, such as percolation and DLA (Diffusion Limited Aggregation) (see companion papers [23], [24] for an application to the present context).

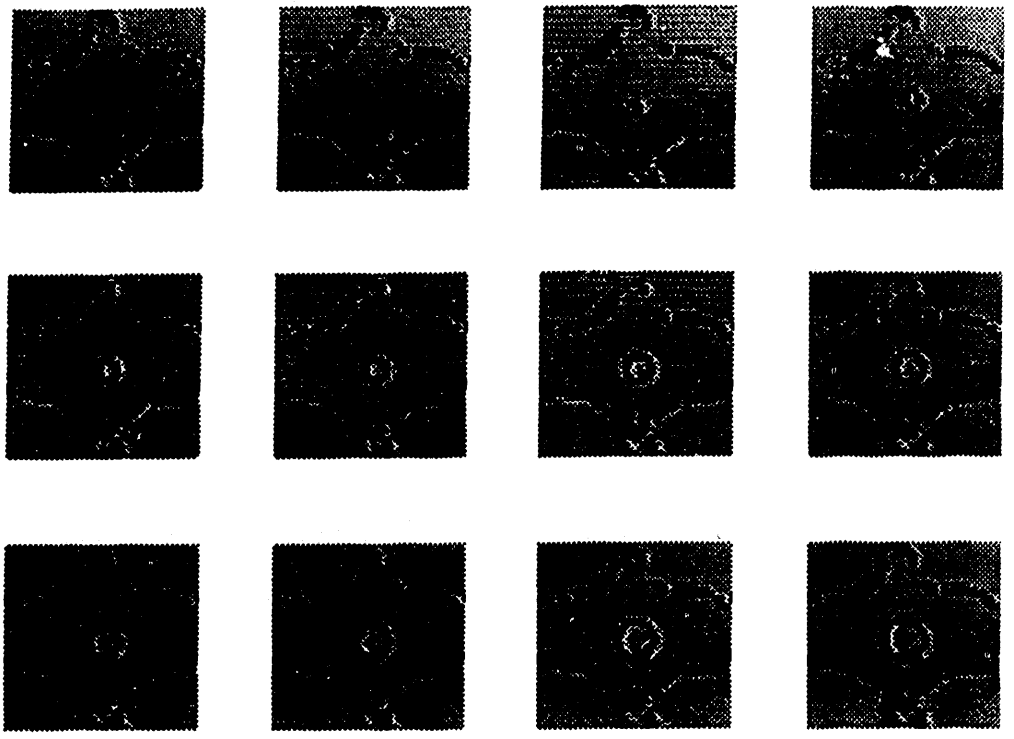

Figure 5. Site activation event (12 snapshots at 1 second intervals).

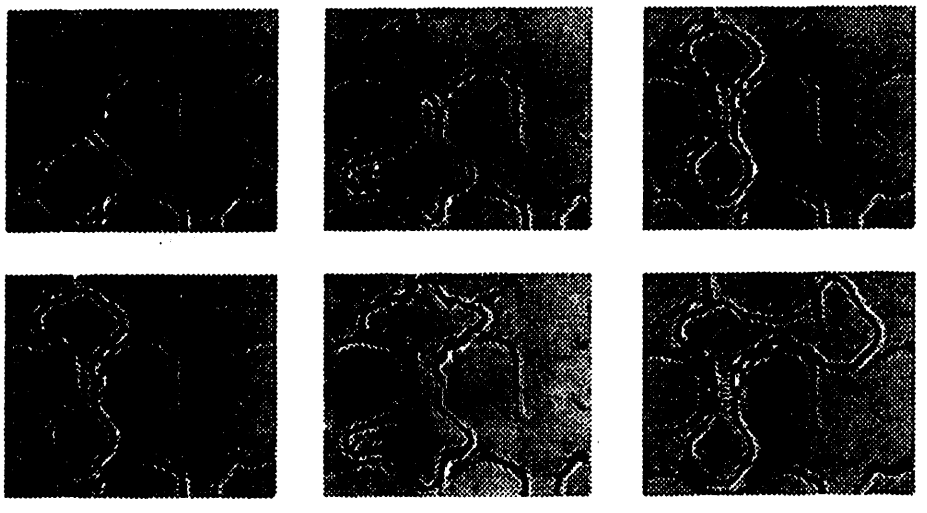

Typical pressure-gas saturation curves at two different pressure decline rates in a 44×24 micromodel are shown in Figure 8. Here, gas saturation denotes the volume fraction of the pore space occupied by the gas. It is shown that as the decline rate increases, the gas saturation corresponding to a given pressure decreases. This is consistent with analogous experiments in laboratory cores,[14] as well as with thenumerical simulations to be shown below. On the other hand, the critical gas saturation, corresponding to the onset of gas flow in the production outlet, was found to be slightly higher in the experiment involving a lower pressure decline rate. This trend is opposite to recent experimental results[9,14,16] (although it must also be noted that Kamath and Boyer[11] observed no significant effect of the pressure decline rate in their low rate experiments). The discrepancy is due to the following: For an unambiguous definition, a critical gas saturation should be identified with the value at which a sample-spanning cluster forms (in a manner similar to a percolation cluster, although here growth also occurs from multiple sites and mass transfer is an additional factor[23,24]). Based on this definition, the theory developed in the companion paper [24] shows that, provided that the nucleation sites are permanently fixed and that nucleation is reproducible, higher pressure decline rates lead indeed to higher critical gas saturations, because of an increase in the number of activated sites. In laboratory experiments, on the other hand, the critical point is ususally identified when gas starts flowing at the outlet of the porous medium. If care is not taken to also ensure that this signals the formation of a sample-spanning cluster, this value would be subject to non-trivial finite-size effects, as it would be significantly affected by the random occurence of some nucleation sites near the production outlet. (In fact, in such cases, the error in the estimation of S_{gc} would increase with its true value). This was the case in our experiments, where the process terminated at the time when gas starts flowing out of the production outlet, even though a sample-spanning cluster is not reached (Figure 4). In addition, in most of our experiments, nucleation events were not reproducible, due to the presence of the coloring dye particles, which frequently acted as nucleation sites. In all such cases, the measured value would actually be a random variable, the sensitivity of which to the pressure decline rate is accordingly subject to uncertainty.

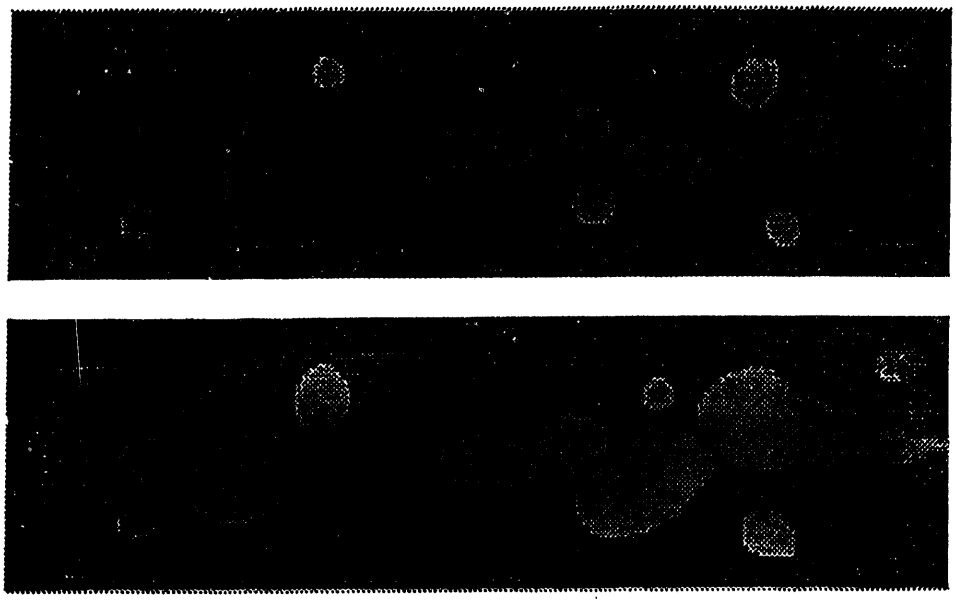

Figure 7. Bubble growth in a Hele-Shaw cell.

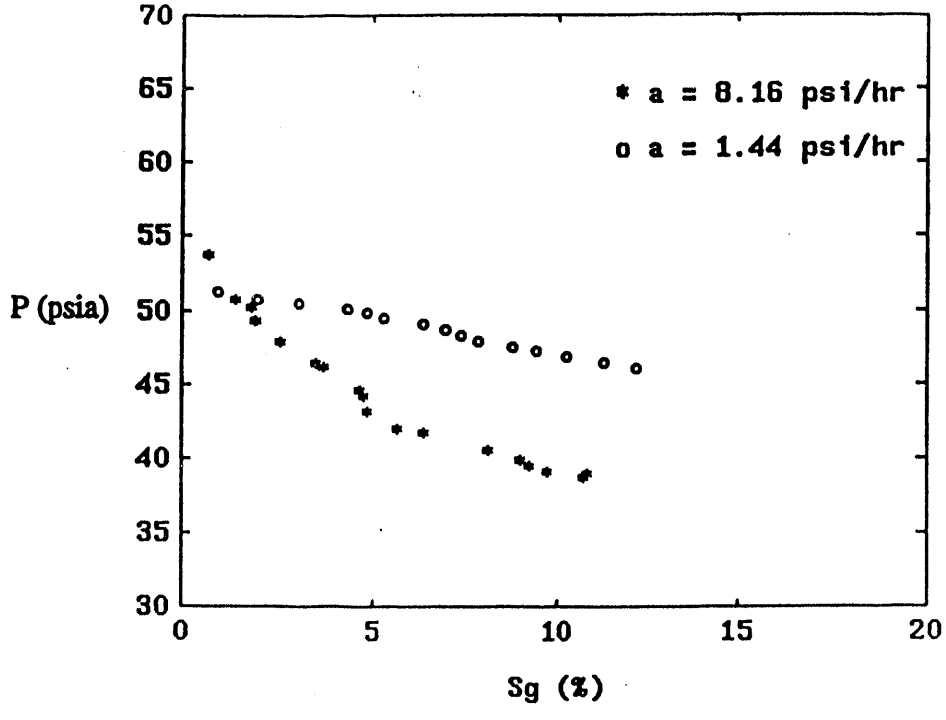

Figure 8. Experimental pressure-saturation curves for two different pressure decline rates.

MATHEMATICAL FORMULATION

To simulate the experiments and to provide a working model for the process, we proceeded with a mathematical formulation. Consider bubble growth in a porous medium, such as the micromodel of Figure 1, the lateral boundaries of which are closed to flow, with the exception of two producing sites at opposites ends. Initially, the medium is occupied by a supersaturated liquid, the pressure of which at the producing side (or in the far-field), $P_{l\infty}$, subsequently declines either at a specified rate $a \equiv -\frac{dP_{l\infty}}{dt}$, or by an abrupt lowering of its value. Constant pressure decline rates are common to many practical applications. To model the nucleation stage, we must specify both the location and the supersaturation level for the activation of nucleation sites. In the simulations of the experiments described below they were determined by direct observation. If a simple cavity model is used (for a detailed discussion, see [31]), site activation requires

$$KC - P_l \geq \frac{2\gamma}{W} \tag{1}$$

where we assumed for simplicity, but without loss in generality, the linear solubility condition

$$P_g = KC \tag{2}$$

between the gas pressure, P_g, and the concentration of the volatile component (dissolved gas) at the gas-liquid interface, C. More generally, one can dispense with a particular model by simply assigning a distribution of nucleation sites at various locations with a distribution of local supersaturations.

Following nucleation, individual gas clusters grow by mass transfer of solute in the liquid-occupied pore space, as described by the usual convection-diffusion equation

$$\frac{\partial C}{\partial t} + \mathbf{u}\cdot\nabla C = D\nabla^2 C \tag{3}$$

where D is the molecular diffusivity. At creeping flow conditions and in the absence of gravity, the liquid velocity $\mathbf{u}$ obeys Stokes' law

$$\nabla P_l = \mu\nabla^2\mathbf{u} \tag{4}$$

(although in the pore network simulations below, momentum balance will be approximated with Poiseuille's law). Despite the fact that pressure gradients and flow velocities are typically quite small, their consideration is necessary in order to account for convection. This has corresponding implications on the complexity of the numerical algorithm. The gas phase is taken isothermal and inviscid, such that the pressure within a connected gas cluster is spatially uiform. Different gas clusters may have different pressures, however. We use the ideal-gas law

$$P_{gk}V_k = n_k RT \tag{5}$$

to relate pressure, P_{gk}, volume, V_k, and mole content, n_k, of a cluster of size k. From the visualization experiments we have observed that cluster growth occurs in two steps. We approximate the pressurizing step with a process of constant V_k and increasing P_{gk}, and the penetration step with a process of constant P_{gk} and increasing V_k. The latter takes place when capillary equilibrium at any gas-liquid interface at the cluster perimeter becomes unstable. Capillary equilibrium is expressed as usual

$$P_{gk} - P_l = \gamma\mathcal{H} \tag{6}$$

where $\mathcal{H}$ is the local curvature. Finally, meniscus displacement is subject to the usual kinematic and mass transfer conditions

$$V_n = \frac{u_n}{1 - \frac{\rho_g}{\rho_l}} \sim u_n \tag{7}$$

and

$$\rho_g(V_n - u_{gn}) = D\frac{\partial C}{\partial n} \tag{8}$$

where V_n, u_n and u_{gn} are the normal components of the interface velocity, the liquid velocity and the gas velocity at the interface, respectively. The determination of u_{gn} requires that the momentum balance in the gas phase be considered. Alternatively, we may proceed by solving only for the integral balance (5) over a given cluster.

The above equations are subject to the appropriate flux or concentration conditions at the boundaries, and to the condition that the concentration on the interface of each cluster is spatially constant. A detailed simulation of the full problem, perhaps with the use of lattice

gas simulation,[32] is not the main scope of this investigation. We will take the simpler, but less accurate, approach of pore network simulation.

PORE NETWORK SIMULATION

Pore network simulators are useful tools for understanding displacements in porous media and have been frequently used in past investigations,[7,33] particularly in immiscible displacement. In such models, the porous medium is represented by an equivalent network of pores of distributed sizes, joined by bonds of another size distribution. Pores are taken to represent the storage capacity of the porous medium, bonds represent flow resistance and provide capillary pressure thresholds. Interfaces are allowed to reside only in pore bodies, the occupancy of which is partial, in general, and dictates the volumetric content of the site. Capillary effects within a pore body are generally not considered. After complete occupancy of the pore body, the meniscus can invade a neighboring pore throat if the corresponding capillary barrier is exceeded. Consistent with these rules, we developed a pore network simulator, where both flow and concentration fields were computed. For a computationally manageable simulation, it was necessary to make certain approximations, such as neglecting the snap-off of gas-liquid interfaces that may occur when certain bonds are penetrated (although such events are rare before the onset of bulk gas flow), and representing invasion as a simplified two-step process. The following rules were used:

1. The network consists of pores and bonds. The pores provide volumetric storage, the bonds control fluid pressure drops and capillary characteristics.

2. Pore bodies can be filled by the gas phase, the liquid phase or both. Pores occupied by liquid can become trapped by gas-occupied pore bodies, if topologically possible. When a pore is trapped, liquid phase movement is not allowed, although diffusion continues.

3. The capillary pressure within a pore body is neglected. The capillary pressure across an interface at the entrance of a bond is inversely proportional to the bond radius.

4. The gas phase is isothermal and inviscid and the gas phase pressure is spatially uniform for all pores belonging to the same cluster, although the gas phase pressure may be

different in different gas clusters.

5. Bond penetration takes place when a pore is fully occupied by gas and the difference between gas and liquid phase pressure exceeds the capillary pressure at the entrance of a bond. There is no limitation on the number of bonds that can be penetrated at each time step.

In the simulations, the governing equations were discretized accordingly. For example, the mass balance for the non-volatile component was expressed as

$$\sum_j Q_{ij} = 0 \tag{9}$$

for site i, where Q_{ij} refers to volume flow rate between adjacent sites i and j. The sum is over all neighboring sites j, and we used Poiseuille's law in place of (3)

$$Q_{ij} = \frac{A_{ij} r_{ij}^2 \Delta P_{ij}}{8\mu l} \tag{10}$$

where A_{ij} is the cross-sectional area of the pore throat joining sites i and j, r_{ij} is the corresponding distributed throat radius and l is the bond length. The mass balance for solute in site i reads

$$(1.0 - S_{gi}) V_s \frac{\Delta C_i}{\Delta t} = \sum_j \left[D A_{ij} \frac{\Delta C_{ij}}{l_{ij}} \right] + \sum_j \left[\frac{A_{ij} r_{ij}^2 \Delta P_{ij}}{8\mu l_{ij}} C_{ij} \right] \tag{11}$$

where V_s is the site volume and S_{gi} is its gas volumetric content ($S_{gi} \neq 0$ if the site happens to belong to the cluster perimeter). Finite increments in time, concentration and pressure were used. The set of equations were solved by an *SOR* method. The computational algorithm is explained in detail in Li[34] and involves the following:

1. Nucleation

Nucleation sites and their supersaturations were distributed at random (or as specified from experimental observations). The host pore body is assumed to become fully occupied by gas immediately after the activation of the nucleation site.

2. Pressurization Step

When all pores in the gas cluster are fully occupied, mass transfer from the liquid to the gas leads to a gas pressure increase, and a throat is eventually invaded. During this step, there is no liquid flow, and the concentration field is determined in the absence of convection. When the smallest capillary pressure threshold at the perimeter is reached, the corresponding bond is penetrated. The time required to complete this process is determined by a trial-and-error procedure.

3. Penetration (Pore-Filling) Step

When partially occupied pores exist in the perimeter of the gas cluster, mass diffusion and (possible) pressure decline eventually lead to their full occupancy. The filling of these pores is carried out in discrete time steps, during which only one of the partially occupied pores becomes fully occupied. The following trial-and-error rules were used:

(a) First, an initial guess for the gas pressure P_{gk} is assumed for each gas cluster, based on which the momentum balance is solved and the liquid pressure field is determined.

(b) Based on the pressure field, the flow rate Q_i at each partially-gas-occupied site i is determined, from which the shortest time to fully occupy one of these sites is found

$$\Delta t_{min} = min_j \left(\frac{V_j}{Q_j} \right) \tag{12}$$

where V_j is the liquid volume displaced from pore j. The volume displaced from each site in the time Δt_{min} is then re-calculated, to yield the overall volume change in the cluster during this step

$$\Delta V_k^{(f)} = \Delta t_{min} \sum_j Q_j \tag{13}$$

where the summation is over all partly occupied perimeter sites.

(c) The corresponding net mass transfer, m_k, into cluster k is next calculated by solving the mass balance equation using the appropriate boundary conditions. The volume change of the gas cluster volume due to mass transfer is then

$$\Delta V_k^{(m)} = \frac{m_k RT}{M_w P_{gk}} - \frac{V_k \Delta P}{P_{gk}} \tag{14}$$

Based on the difference between $\Delta V_k^{(f)}$ and $\Delta V_k^{(m)}$ additional iterations are taken on the assumed gas pressure until convergence is reached. Finally, at the end of each time step, a check is made to determine if any new nucleation sites are activated and to determine whether conditions exist for additional perimeter throats to be penetrated.

SIMULATION OF EXPERIMENTAL RESULTS

To test the validity of the simulator, the glass micromodel experiments were simulated. The geometry of the network used in the simulation is the same with the computer pattern used to construct the glass micromodel. However, the true sizes of the micromodel pores are likely to be somewhat different due to various defects during the fabrication process, as explained above. For each experiment simulated, information from the actually observed nucleation events (location and time) was used as input to the numerical model. Because of the 2-D nature of the micromodel, the pores and throats were approximated as equivalent rectangular plates and channels. Even though the etching depth of the glass micromodel is unknown, this value do not affect significantly the simulation results, because they affect site volumes and mass transfer areas in equal proportions. For calculation purposes, a vaule of 500 μm was used in all simulations.

The following values were assigned to the physical variables: $\mu = 1\ cp$, $\gamma = 72\ dyne/cm$, $T = 530\ ^oF$ and $M_w = 44$. The solubility parameters were estimated from the data reported in [35]. The gas solubility constant K was calculated to be 8820 psi/gcm^3. All experiments were carried out at the initial pressure of 71.4 $psia$, corresponding to an initial concentration of 0.0081 g/cm^3. Diffusion coefficients of CO_2 in water were reported in the range 1.0×10^{-5} to $3.0 \times 10^{-5}\ cm^2/s$.[36] The effect of the diffusivity on the process is quite important. Shown in Figure 9a is a plot of the simulation of an experiment at the low pressure decline rate of 1.44 psi/hr, during which 10 nucleation sites were activated. Since a diffusivity value was not actually measured, we selected the value of $3.0 \times 10^{-5}\ cm^2/s$, which best fitted this experiment. The value is consistent with the published data. The corresponding simulated cluster pattern is shown in Figure 9b. Such patterns are typical of the growth

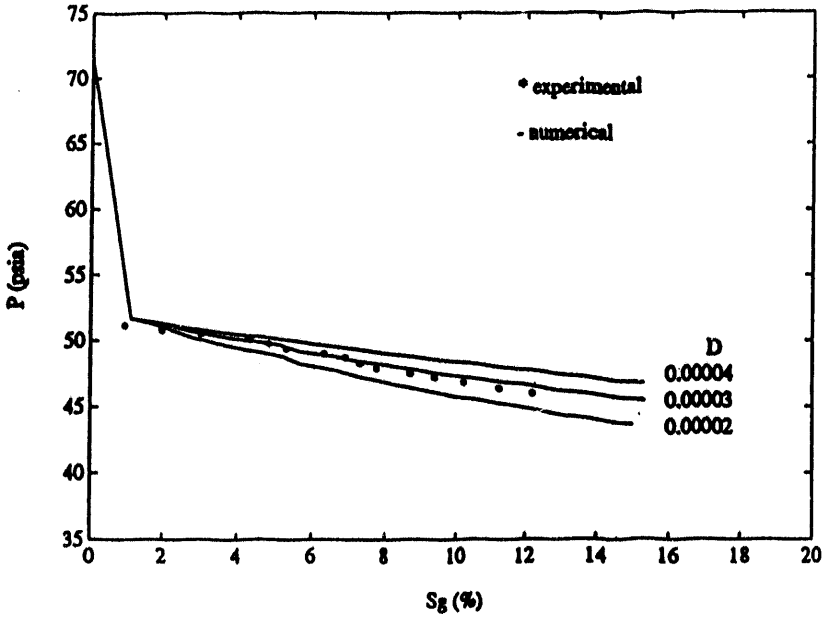

(a) Pressure-saturation curves at different values of *D*.

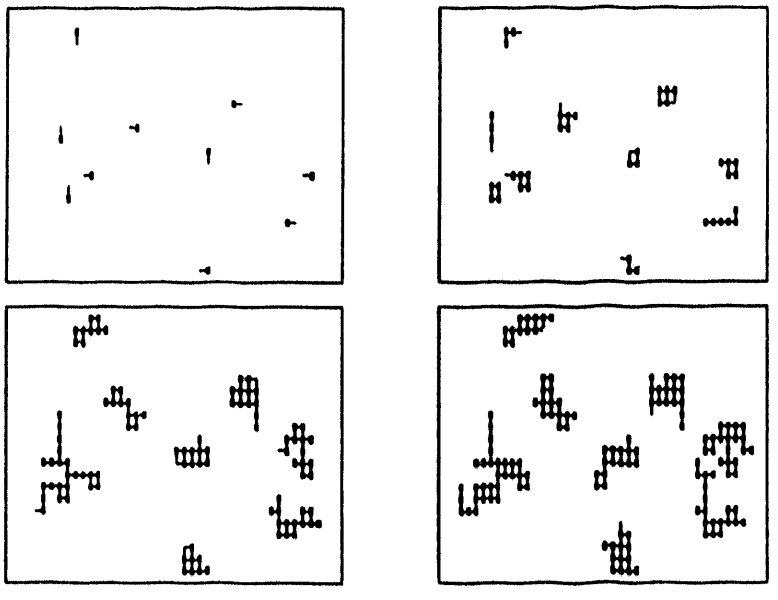

(b) Simulated gas cluster pattern

Figure 9. Pore network simulation of experimental result s (a = 1.44 psi/hour).

patterns generated by the numerical algorithm. Based on the above parameter values and on the original network pattern, we tested the simulator for various experiments conducted in two different glass micromodels of sizes 44 × 24 and 65 × 35, respectively. Several runs at different pressure decline rates with varying nucleation fractions were conducted and simulated. Additional details can be found in Li.[34]

Experimental and simulated results of pressure-saturation curves, which represent the overall system behavior, as well as of growth patterns, which provide local detail, were compared. Figure 10 shows four different pressure-saturation curves conducted at different pressure decline rates. A good agreement between experiments and simulations is noted. Some discrepancy exists at the latter stages of the process for $a = 8.16 psi/hr$, where the numerical results tend to overestimate the saturations. However, given the simplified nature of the numerical model, the uncertainty in the actual geometry of the pattern, and the fact that no adjustable parameters were used, the agreement is quite acceptable.

We should point out that a different number of nucleation sites were activated during these processes. In fact, because of the uncertainty in the nucleation process for the reasons previously cited, the frequency of nucleation did not follow the expected, for permanently fixed sites, trend of increasing with increases in a. For example, an activation of 5, 7, 10 and 5 sites was observed in the experiments with pressure decline rates equal to 8.64, 3.96, 1.44 and 8.16 psi/hr, respectively. As a result, definitive conclusions about the effect of a are not possible from these experiments, where nucleation is not reproducible. For fixed nucleation sites activated at different supersaturations, however, a sensitivity study using the numerical simulator and a theoretical analysis[24] show that the effect of a is to lead to lower gas saturation for the same pressure at higher values of a (which is also consistent with Figure 8). A more stringent test of the simulator isto compare local growth patterns. Figure 11 shows the comparison between the experimental and numerical patterns for one of the experiments. The two patterns share many similar characteristics, although the patterns are not identical. To some extent, this is to be anticipated, in view of the incomplete knowledge of the geometrical structure of the micromodel. Indeed, it is uncertain whether the capillary characteristics of the micromodel and the numerical model are identical. This produces different occupancy sequences, therefore ndifferent growth patterns, in the two models. For

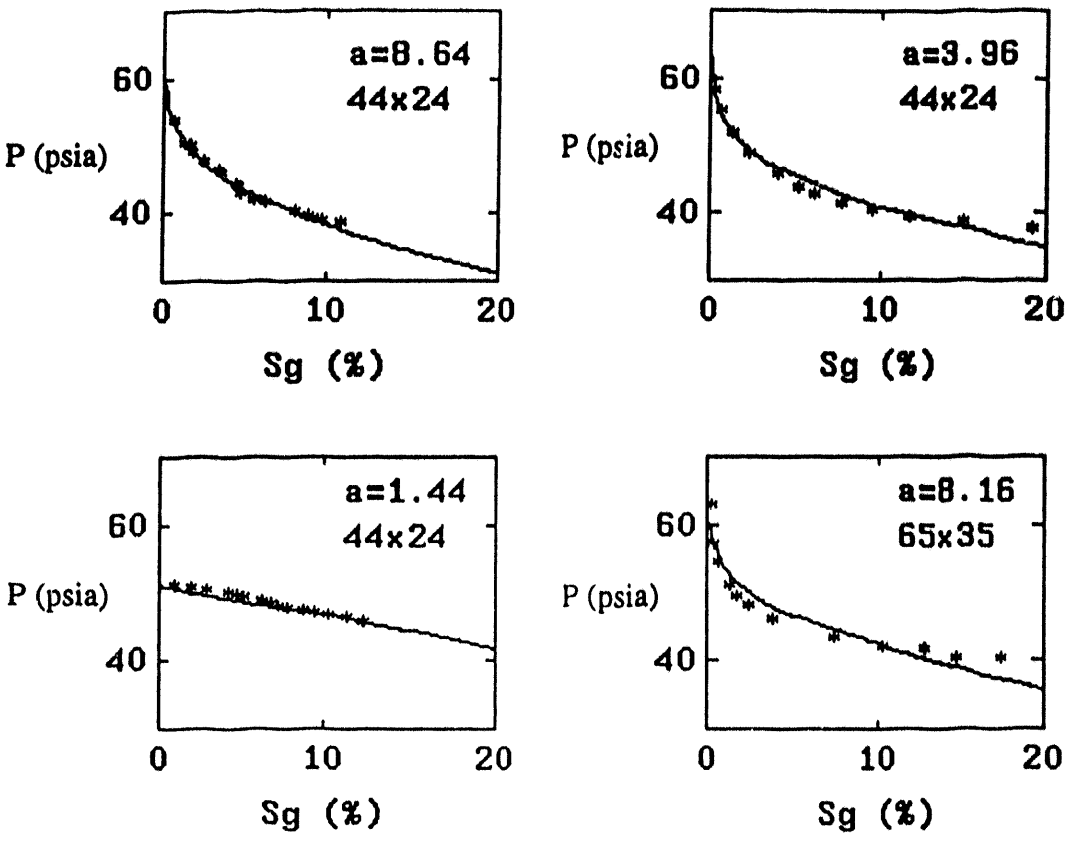

Figure 10. Comparison between experimental and pore network simulated P-S_g curves.

the same reasons, a precise agreement between experimental and simulated patterns has not been obtained, to our knowledge, even in simpler external displacements, such as drainage. This uncertainty precludes the simulator from accurately matching the microscopic details in the more complex process of bubble growth. On the other hand, the experimentally observed "one-throat-at-a-time" growth mode was exactly matched during the simulation, indicating that the dominant mechanism was correctly simulated. These simulations have revealed that although the overall patterns are not in the global percolation regime, individual clusters still obey *local percolation* rules. Overall, the good agreement in matching the overall behavior is encouraging of the ability of the simulator to match important aspects of phase growth. The companion papers [23], [24] show how the simulator was used in the development of some simple theories and statistical models for bubble growth, in the delineation of patterns and rates of growth and in assessing the effect of nucleation. In particular, the important issues of the critical gas saturation and pressure decline rate are systematically investigated.

CONCLUSIONS

In this paper, we conducted visualization ex periments of bubble growth in glass micromodels taken to represent model porous media. The experiments confirmed many of the premises taken previously,[17] namely the onset of nucleation from different sites, the growth of vapor clusters in a ramified, rather than a compact, fashion, and the relevance of capillary effects to the growth process. The latter dictate a two-step growth mechanism, which at low and moderate pressure decline rates, occurs "one-throat-at-a-time". These experimental observations were subsequently incorporated into a pore network model, which includes nucleation, growth by mass transfer and viscous and capillary effects. Numerical simulation of the experiments showed a good agreement in the overall features, but a poorer agreement in the microscale details. We attributed the latter to the uncertainty in the precise structure of the micromodel. The results were also consistent with simpler analytical results in the limit of slow growth. In the latter case, the relevance of a percolation approach to describe the growth process was verified. In particular, at the decline rates studied, local percolation rules also dictate the growth of each individual cluster. However, when many nucleation clusters are involved, their competition for solute results into a pore occupancy sequence different

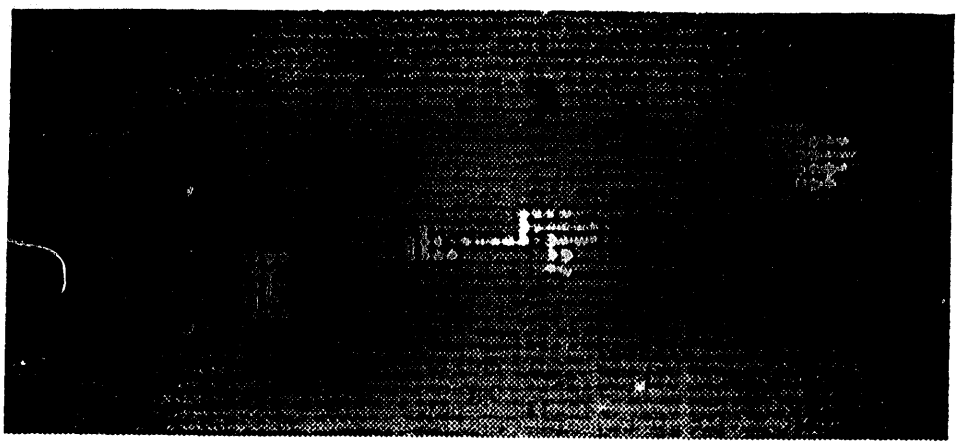

(a) Experimental

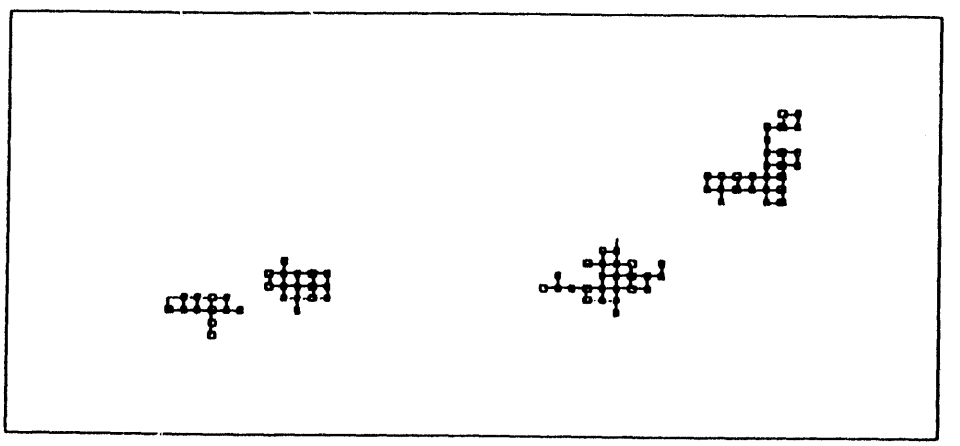

(b) Pore network simulation

Figure 11. Comparison of local cluster growth patterns for a = 5.24 psi/hr.

than global percolation. The simulator was successfully used to explore various aspects of bubble growth as described in the companion papers [23], [24].

ACKNOWLEDGEMENTS

This work was partly supported by a grant from Chevron Oil Field Research (now Chevron Petroleum Technology Corporation). Additional support was provided by the USC Center for the Study of Fractured Reservoirs, supported by Aramco, Mineral Management Services, State Lands Commission of California, Texaco E & P and Unocal Science & Technology. All these sources of support are gratefully acknowledged. Useful discussions with Jairam Kamath are also acknowledged.

NOMENCLATURE

A_k = Surface area of cluster k

[D a = Pressure decline rate

C = Concentration of solute (dissolved gas)

C_{Dk} = Dimensionless interface concentration of cluster k

Ca = Capillary number

C_0 = Initial concentration of solute

C_∞ = Far-field concentration of solute

D = Diffusion coefficient

D_f = Fractal dimension

f_q = Nucleation fraction

Ja = Jacob number

K = Solubility constant

k = Permeability

L = Pore network dimension

l = Length

l^* = Characteristic length

M_w = Molecular weight

n_k = Mole fraction of cluster k

P = Pressure

P_0 = Initial system pressure

P_∞ = Far-field system pressure

Q = Liquid withdrawal rate

R = Radius of gyration

R^p = Critical size of percolation

REFERENCES

1. Hunt, E.B. Jr., and Berry, V.J. Jr.: "Evolution of Gas from Liquids Flowing through Porous Media", *AIChE J* 560-567 (1956).

2. Thome, J. R., *Enhanced Boiling Heat Transfer*, Hemisphere Publishing Co. (1990).

3. Schubert, G. and Strauss, J. M.: "Two-Phase Convection in a Porous Medium", *J. Geophys. Res.* **82**, 3411-3421 (1977).

4. Doughty, C. and Pruess, K.: "A Semianalytical Solution for Heat-Pipe Effects Near High-Level Nuclear Waste Packages Burried in Partially Saturated Geological Media", *Int. J. Heat Mass Transfer* **31**, 79-90 (1988).

5. Scriven, L.E.: "On the Dynamics of Phase Growth", *Chem. Eng. Sci.* **10**, 1-13 (1959).

6. Plesset, M.S. and Prosperetti, A.: "Bubble Dynamics and Cavitation", *Ann. Rev. Fluid Mech.* **9**, 145-185 (1977).

7. Lenormand, R., Touboul, E. and Zarcone, C.: "Numerical Models and Experiments on Immiscible Displacements in Porous Media", *J. Fluid Mech.*, **189**, 165-187 (1988).

8. De Swaan, A.: "Development of the Critical Gas Saturation", *JPT* 907-908 (1981).

9. Firoozabadi, A., Ottesen, B. and Mikklesen, M.: "Measurement and Modeling of Supersaturation and Critical Gas Saturation: Part 1, Measurements", paper SPE 19694 presented at the 64th SPE Annual Fall Meeting, San Antonio, TX (Oct. 8-11, 1989).

10. Li, X. and Yortsos, Y. C.: "Critical Gas Saturation: Modeling and Sensitivity Study," paper SPE 26662 presented at the 68th SPE Annual Fall Meeting, Houston, TX (Oct. 3-6, 1993).

11. Kamath, J. and Boyer, R. E.: "Critical Gas Saturation and Supersaturation in Low Permeability Rocks" paper SPE 26663 presented at the 68th SPE Annual Fall Meeting, Houston, TX (Oct. 3-6, 1993).

12. Satik, C., *Ph.D Dissertation*, University of Southern California (1993).

13. Moulu, J. C. and Longeron, D.: "Solution-Gas Drive: Experiments and Simulation", paper presented at the fifth European Symposium on Improved Oil Recovery, Budapest, Hungary (April 5-7, 1989).

14. Kortekaas, T.F.M. and Poelgeest, F.V.: "Liberation of Solution Gas During Pressure Depletion of Virgin and Watered-Out Reservoirs", paper SPE 19693 presented at the 64th SPE Annual Fall Meeting, San Antonio, TX (Oct. 8-11, 1989).

15. Kashchiev D. and Firoozabadi A.: "Kinetics of the Initial Stage of Isothermal Gas Phase Formation", *J. Chem. Phys.* **98**, 1-15 (1993).

16. Kashchiev D. and Firoozabadi A.: "Pressure and Volume Evolution During Gas Phase Formation in Solution Gas Drive Process", paper SPE 26286, preprint (1993).

17. Yortsos, Y. C. and Parlar, M.: "Phase Change in Binary Systems in Porous Media: Application to Solution Gas Drive," paper SPE 19697 presented at the 64th SPE Annual Fall Meeting, San Antonio, TX (Oct. 8-11, 1989); revised paper submitted to *Chem. Eng. Sci.* (1993).

18. Yousfi, El., Zarcone, C., Bories, S. and Lenormand, R.: "Mechanisms of Solution Gas Liberation during Pressure Depletion in Porous Media", *C. R. Acad. Sci. Paris*, t. **313**, Serie II, 1093-1098 (1991).

19. Yousfi, El., Zarcone, C., Bories, S. and Lenormand, R., poster paper presented at the 5th IFP Research Conference, Arles, France (1990).

20. Danesh, A., Peden, J.M., Krinis, D. and Henderson, G.D.: "Pore Level Visual Investigation of Oil Recovery by Solution Gas Drive and Gas Injection", paper SPE 16956 presented at the 62nd SPE Annual Fall Meeting, Dallas, TX (Sep. 27-30, 1987).

21. Lifshitz, I. M., and Slyozov, V. V.: "The Kinetics of Precipitation from Supersaturated Solid Solutions", *J. Phys. Chem. Solids*, **19**, 35-50 (1961).

22. Li, X. and Yortsos, Y. C.: "Bubble Growth and Stability in an Effective Porous Medium", *Phys. Fluids A*, submitted (1993).

23. Satik, C., Li, X. and Yortsos, Y. C.: "Scaling of Bubble Growth in Porous Media", *Phys. Rev. Lett.*, submitted (1993).

24. Li, X. and Yortsos, Y. C.: "Bubble Growth in Porous Media", *Chem Eng. Sci.*, submitted (1993).

25. Chatzis, I.: "Photofabrication Technique of 2-D Glass Micromodels", PRRC Report No. 82-12, New Mexico Institute of Technology (1982).

26. Kennedy, H.T. and Olson, C.R.: "Bubble Formation in Supersaturated Hydrocarbon Mixtures", *Trans. AIME* **195**, 271-8 (1952).

27. Stewart, C.R., Hunt, E.B. Jr., Schneider, F.N., Geffen T. M. and Berry, V.J. Jr.: "The Role of Bubble Formation in Oil Recovery by Solution Gas Drives in Limestones", *Trans. AIME* **201**, 294-301 (1954).

28. Wieland, D.R. and Kennedy, H.T.: "Measurement of Bubble Frequency in Cores", *Trans. AIME* **210**, 123-5 (1957).

29. Payatakes, A.C. and Dias, M. M.: "Immiscible Microdisplacement and Ganglion Dynamics in Porous Media", *Rev. in Chem. Eng.* **2**, 85-174 (1984).

30. Homsy, G.M.: "Viscous Fingering in Porous Media", *Ann. Rev. Fluid Mech.* **19**, 271-311 (1987).

31. Atchley, A.A. and Prosperetti, A.: "The Crevice Model of Bubble Nucleation", *J. Acoust. Soc. Am.* **86**, 1065-1084 (1989).

32. Rothman, D. H.: "Cellular-automaton Fluids: A Model for Flow in Porous Media", *Geophys.* **53**, 509-518 (1988).

33. Blunt, M. and King, P.: "Relative Permeabilities from Two- and Three-Dimensional Pore-Scale Network Modelling", *Transport in Porous Media* **6**, 407-433 (1991).

34. Li, X.: "Bubble Growth during Pressure Depletion in Porous Media", *Ph.D Dissertation*, University of Southern California (1993).

35. Quinn, E. L. and Jones, C. L., *Carbon Dioxide*, Reinhold, New York (1936).

36. Vivian, J. E. and King, C. J.: "Diffusivities of Slightly Soluble Gases in Water", *AIChE J.* **10**, 220 (1964).

☆U.S. GOVERNMENT PRINTING OFFICE: 1994 - 560-030/00002

END

DATE
FILMED
3/29/94